essential. Indeed, experimental design in multivariate calibration is an extensive subject in itself (*41*, *42*).

Multivariate calibration approaches other than MLR and PCR might be preferred under certain circumstances; for example, GSAM would be useful in situations where the MO^+/M^+ values are matrix-dependent, or if a high dissolved solids content produced large differences in analyte sensitivity between sample and standard solutions. GSAM may also be practical where only a few samples are involved, as no external calibration is performed. The partial least-squares method (PLS) has been successfully applied to underdetermined systems (*31*), i.e. those systems where fewer sensors than analytes exist. PLS may be useful in some situations such as the determination of As and Se in soil digestates, where a complex variety of oxygen-, chlorine-, potassium-, and argon-containing molecular species may cause problems.

LITERATURE CITED

(1) Gray, A. L. *Analyst* **1975**, *100*, 289-299.
(2) Houk, R. S.; Fassel, V. A.; Flesch, G. D.; Svec, H. J.; Gray, A. L.; Taylor, C. E. *Anal. Chem.* **1980**, *52*, 2283-2289.
(3) Date, A. R.; Gray, A. L. *Analyst* **1981**, *106*, 1255-1267.
(4) Date, A. R.; Gray, A. L. *Analyst* **1983**, *108*, 159-165.
(5) Date, A. R.; Gray, A. L. *Int. J. Mass Spectrom. Ion Phys.* **1983**, *46*, 7-10.
(6) Date, A. R.; Gray, A. L. *Spectrochim. Acta* **1983**, *38B*, 29-37.
(7) Gray, A. L.; Date, A. R. *Analyst* **1983**, *108*, 1033-1050.
(8) Gray, A. L.; Date, A. R. *Int. J. Mass Spectrom. Ion Phys.* **1983**, *48*, 357-360.
(9) Date, A. R.; Gray, A. L. *Spectrochim. Acta* **1985**, *40B*, 115-122.
(10) Olivares, J. A.; Houk, R. S. *Anal. Chem.* **1985**, *57*, 2674-2679.
(11) Houk, R. S.; Svec, H. J.; Fassel, V. A. *Appl. Spectrosc.* **1981**, *35*, 380-384.
(12) Douglas, D. J.; Quan, E. S. K.; Smith, R. G. *Spectrochim. Acta* **1983**, *38B*, 39-48.
(13) Doherty, W.; Vander Voet, A. *Can. J. Spectros.* **1985**, *30*, 135-141.
(14) Douglas, D. J.; Houk, R. S. *Prog. Anal. At. Spectrom.* **1985**, *8*, 1-18.
(15) Gray, A. L. *J. Anal. At. Spectrom.* **1986**, *1*, 247-249.
(16) McLeod, C. W.; Date, A. R.; Cheung, Y. Y. *Spectrochim. Acta* **1986**, *41B*, 169-174.
(17) Vaughn, M. A.; Horlick, G. *Appl. Spectrosc.* **1986**, *40*, 434-445.
(18) Date, A. R.; Cheung, Y. Y.; Stuart, M. E. *Spectrochim. Acta* **1987**, *42B*, 3-20.
(19) Gray, A. L.; Williams, J. G. *J. Anal. At. Spectrom.* **1987**, *2*, 81, 82.
(20) Horlick, G.; Tan, S. H.; Vaughn, M. A.; Rose, C. A. *Spectrochim. Acta* **1985**, *40B* 1555-1572.
(21) Hutton, R. C.; Eaton, A. N. *J. Anal. At. Spectrom.* **1987**, *2*, 595-598.
(22) Lichte, F. E.; Meier, A. L.; Crock, J. G. *Anal. Chem.* **1987**, *59*, 1150-1157.
(23) Saxberg, B. E. H.; Kowalski, B. R. *Anal. Chem.* **1979**, *51*, 1031-1038.
(24) Jochum, C.; Jochum, P.; Kowalski, B. R. *Anal. Chem.* **1981**, *53*, 85-92.
(25) Kalivas, J. H.; Kowalski, B. R. *Anal. Chem.* **1981**, *53*, 2207-2212.
(26) Kalivas, J. H.; Kowalski, B. R. *Anal. Chem.* **1982**, *54*, 560-565.
(27) Gerlach, R. W.; Kowalski, B. R. *Anal. Chim. Acta* **1982**, *134*, 119-127.
(28) Kalivas, J. H. *Anal. Chem.* **1983**, *55*, 565-567.
(29) Lindberg, W.; Persson, J. A.; Wold, S. *Anal. Chem.* **1983**, *55*, 643-648.
(30) Sjostrom, M.; Wold, S.; Lindberg, W.; Persson, J.; Martens, H. *Anal. Chim. Acta* **1983**, *150*, 61-70.
(31) Frank, I. E.; Kalivas, J. H.; Kowalski, B. R. *Anal. Chem.* **1983**, *55*, 1800-1804.
(32) Mandel, J. *Am. Stat.* **1982**, *36*, 15-24.
(33) Cowe, I. A.; McNicol, J. W. *Appl. Spectrosc.* **1985**, *39*, 257-266.
(34) Fredericks, P. M.; Lee, J. B.; Osborn, P. R.; Swinkels, D. A. J. *Appl. Spectrosc.* **1985**, *39*, 303-310.
(35) Gemperline, P. J.; Boyette, S. E.; Tyndall, K. *Appl. Spectrosc.* **1987**, *41*, 454-459.
(36) Donahue, S. M.; Brown, C. W.; Caputo, B.; Modell, M. D.; *Anal. Chem.* **1988**, *60*, 1873-1878.
(37) Beebe, K. R.; Kowalski, B. R. *Anal. Chem.* **1987**, *59*, 1007A-1017A.
(38) Deming, S. N.; Morgan, S. L. *Experimental Design: A Chemometric Approach*; Elsevier: Amsterdam, 1987; Chapter 9.
(39) Currie, L. A. *ACS Symp. Ser.* **1988**, No. 361, 1-62.
(40) Delaney, M. F. *Anal. Chem.* **1984**, *56*, 261R-277R.
(41) Mark, H. *Anal. Chem.* **1986**, *58*, 2814-2819.
(42) Cahn, F.; Compton, S. *Appl. Spectrosc.* **1988**, *42*, 856-872.

RECEIVED for review January 27, 1989. Accepted June 20, 1989. This work was supported by the U.S. Environmental Protection Agency. Mention of specific suppliers and products is for information purposes only and does not constitute official endorsement.

Ion Detection by Fourier Transform Ion Cyclotron Resonance: The Effect of Initial Radial Velocity on the Coherent Ion Packet

Curtiss D. Hanson, Eric L. Kerley, Mauro E. Castro, and David H. Russell*

Department of Chemistry, Texas A&M University, College Station, Texas 77843

Ion detection by Fourier transform ion cyclotron resonance (FT-ICR) is accomplished by observing a coherent ion packet produced from an initially random ensemble of ions. The coherent packet is formed by excitation with a resonant oscillating electric field. Ions that are out of phase with the applied radio frequency (rf) electric field experience a continuous misalignment of the electric field vector. The misalignment creates a net force of the electric field perpendicular to ion motion. The perpendicular component of the rf electric field creates a frequency shift resulting in phase synchronization of the ion ensemble. The phase coherence of the ion packet affects both the sensitivity and the resolution of FT-ICR.

INTRODUCTION

Over the past decade, there has been rapid development in Fourier transform ion cyclotron resonance (FT-ICR). As noted in several reviews (*1-10*), the growth in FT-ICR can be attributed to the performance characteristics of the instrument (i.e., the ability to perform high-resolution mass measurements, the extended mass range (m/z >10 000) (*11*, *12*), and the ability to perform high-resolution mass measurements at high mass). FT-ICR had its foundation in the concept of the ion trap. The ability to store ions for long periods of time (milliseconds to seconds), provides a high degree of flexibility in terms of ion manipulation and detection. For example, ion storage permits both high sensitivity and versatility required to perform tandem mass spectrometry (MS) experiments (e.g., photodissociation (*13*) and collision induced dissociation (CID) (*14*, *15*)).

Ion cyclotron resonance was developed during the mid 1960s (*16*), based on work performed a decade before (*17-19*), primarily for studying ion-molecule reactions. During this period the major emphasis was placed on the development of mass analysis techniques. The principal method of sample ionization was electron impact which produces ions having near thermal kinetic energies. Thus, the mass analysis

0003-2700/89/0361-2040$01.50/0

techniques that evolved during this period were designed and developed for ions for low translational energies.

Recent advancements in "soft" ionization methods which are suitable for nonvolatile, thermally labile, and polar compounds (viz., fast atom bombardment (FAB) (*20*), secondary ion mass spectrometry (SIMS) (*21*), and laser desorption (*22*)) have greatly expanded the scope of mass spectrometry. Although these ionization methods have been adapted for use with FT-ICR (*23*, *24*) and are capable of producing intact molecular ions, the kinetic energies (>thermal) imparted to the sample ions can have adverse effects on the instrument performance. In order to realize the theoretical potential of FT-ICR, the effect of initial ion kinetic energy on ion trapping and detection must be evaluated. Further, developments in FT-ICR must be based on a thorough understanding of the dynamics of the ion trap. Specifically, the effect of the crossed electric and magnetic fields on ion trajectories in the ICR cell, as well as the impact of ion motion and ion energy on detection, requires further investigation. Although there has been much success in FT-ICR since its introduction by Comisarow and Marshall (*25*), the theoretical performance (*26*, *27*) has only been realized for a relatively narrow range of operating conditions (e.g., ions produced by electron impact with low translational energies). Extending the operating mass range of FT-ICR to include high molecular weight biomolecules (>2500 amu) revealed fundamental problems with mass analysis by FT-ICR, viz., the inability to perform high-resolution mass measurement at high mass (*12*, *28*, *29*). Although impressive mass resolution has been recorded for small peptides which can be efficiently ionized (and therefore produce a large number of intact molecular ions) the short duration of the time-domain transient signal for peptide ions above 2000 daltons seriously limits high-resolution mass measurements. Recently Wilkins and co-workers reported high-resolution data for high mass ions formed by laser desorption. These results differ from other analysis methods in that the ions studied are nonpolar organic polymers, and laser desorption produces a high abundance of ions and neutrals. The high yield for ions and neutrals can result in both ion/ion and ion/neutral relaxation processes (*30*, *31*), which potentially quench radial and axial ion motion and improve both ion trapping (sensitivity) and mass resolution.

Ion detection by FT-ICR is accomplished by observing the image current produced by a coherent ion packet. Therefore, the performance characteristics associated with the technique arise from the ability to produce synchronous ion motion from an ensemble of ions having random initial velocities and ICR orbital phase angles (*32*, *33*). A coherent packet of ions is defined by an ensemble of ions which can be presented by a rotating monopole. To meet this requirement the ion ensemble must be spatially well-defined. Spatial definition is a combination of radial distribution (i.e., energy distribution) and radial dispersion (i.e., phase relationship). Signal intensity and resolution are dependent upon the spatial distribution of the ensemble and the length of time the packet is observed. Loss of signal or resolution in FT-ICR is, therefore, attributed to the loss of coherent ion motion (*34*).

In this paper we examine several factors that influence the production of a coherent ion packet. The effect of random initial phases on the final translational energy distribution (i.e., radial distribution) was recognized early in the development of ICR (*35–37*), but because of the low magnetic fields used (ca. 0.7–0.9 T) and thermal ion kinetic energies (e.g., kinetic energies of ions produced by electron impact) the effect of the phase angle on the production of a coherent ion packet was negligible. Clearly such considerations are different today; the high mass FT-ICR instruments use high magnetic fields (3–7 T) and external ion sources which impart significant translational energies to the ions. Under these conditions the effect of the ions phase angle is no longer insignificant and cannot be neglected.

The effects of ion motion and phase angle are difficult to study in a simple cubic ICR cell. Although the two-section ion cell was initially developed to deal with the FT-ICR requirements of ion detection at high vacuum (*38*), the work presented in this paper illustrates the flexibility of this cell to address problems of ion motion and the dynamics of ion detection. This paper examines the nonideal effects on ion motion resulting from (i) significant radial translational energy (>thermal), (ii) initially random phase angles, and (iii) the process that leads to phase synchronous motion of an initially random ion population. Experimental results from two-section ion cell studies and theoretical ion trajectories determined by numerical computer solution of the equation of ion motion are used to examine the effects of initial radial velocity on the ability to create coherent ion motion.

EXPERIMENTAL SECTION

All experiments were performed on a prototype Nicolet Analytical Instruments FTMS-1000 spectrometer equipped with a 3-T superconducting magnet. The vacuum system has been modified to accommodate a two-section cell (*39*, *40*). The two-section cell consists of two cubic cells (3.81 × 3.81 × 0.81 cm) mounted collinearly along the central axis of the magnetic field. The two cells share a common trap plate that also serves as a conductance limit for the differential pumping system. The aperture in the conductance limit has a radius of 2 mm. The vacuum in both sections of the differentially pumped system is maintained by oil diffusion pumps. Background pressures for both sections of the vacuum system were 1×10^{-8} Torr or less. Gaseous reagents are admitted to the vacuum system by variable leak valves (Varian Series 951) and maintained at 2×10^{-7} Torr. Ionization was performed by electron impact (50-eV electrons, 200 nA). Detection of the ions in either the source or the analyzer region of the cell was performed by electronically switching the rf excite pulses between the cell regions.

RESULTS AND DISCUSSION

The motion of a charged particle in a magnetic field (B) is constrained to a circular orbit of angular frequency (ω) in a plane perpendicular to the magnetic field lines. The Lorentz force ($qv_{xy}B$) acting on the ion is directly proportional to the ion's velocity perpendicular to the magnetic field, v_{xy} (i.e., the component of the velocity vector in the $X-Y$ plane). The radius of the cyclotron orbit is obtained by equating the Lorentz force to the centrifugal force. Because the frequency of the cyclotron motion is inversely proportional to mass (m), the mass-to-charge value (m/z) of an ion can be determined by measuring the frequency of the cyclotron motion in a static magnetic field.

Having introduced the rudiments of ion motion in the FT-ICR experiment, it is necessary to consider the problems arising in ion trapping and ion detection in experiments involving (i) the ideal case where ions with thermal kinetic energies are *trapped* in the center of the ion cell (e.g., electron impact ionization) and (ii) the case where ions with significant translational energies are *stored* in the ion cell (e.g., ions formed by FAB, SIMS, or laser desorption mass spectrometry (LDMS) within the cell or injected from external ion sources).

In a typical electron impact ionization FT-ICR experiment, ions are formed over a period of several milliseconds (many cyclotron orbits) from neutrals having random motions. Ion formation therefore results in an initial ensemble of ions which is phase incoherent. The initial translational energy of the ion population corresponds to the thermal kinetic energy distribution of the neutrals prior to ionization. Because the ions are formed from the neutral molecules have random velocity vectors with respect to the direction of the magnetic field, the original theoretical development of FT-ICR was

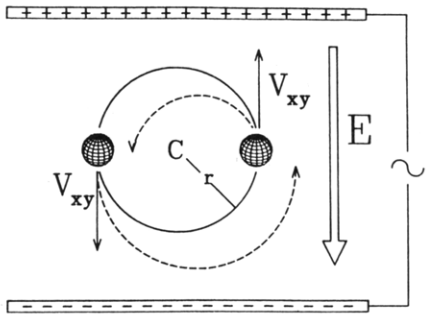

Figure 1. Trajectories for two ions having the same angular frequency but different phase being accelerated by a resonant rf electric field. An ion which is inphase and resonant with the applied rf electric field is accelerated to a larger cyclotron radius. Conversely, an ion which is out of phase is decelerated to lower translational energies and therefore a smaller cyclotron radius.

based on an initial ion population having subthermal energies.

The mechanism for creation of a coherent packet of ions is acceleration by a resonant oscillating electric field (i.e., rf irradiation). Ions of a given m/z ratio are continuously accelerated by rf electric potential gradients which are inphase with the ion's motion. Ions that have an initial random phase relationship with respect to the oscillating electric field must be forced into phase coherence prior to a net acceleration (*41*). Therefore, an ion must be both (i) resonant with and (ii) inphase with the applied rf field to acquire translational energy.

The excitation rf field can be described as a sum of two phase-related contrarotating electric fields (*35*).

$$\mathbf{E}(t)_{sum} = \mathbf{E} \sin(\omega t) = \mathbf{E}^{+}(t) + \mathbf{E}^{-}(t) \quad (1)$$

where

$$\mathbf{E}^{+}(t) = (1/2)\,\mathbf{E}(\sin \omega t\mathbf{i} + \cos \omega t\mathbf{j}) \quad (2)$$

$$\mathbf{E}^{-}(t) = (1/2)\,\mathbf{E}(\sin \omega t\mathbf{i} - \cos \omega t\mathbf{j}) \quad (3)$$

The sum of the components results in an electric field which has magnitude and direction. The frequency of the resultant oscillating electric field (ω_{rf}) is determined by the period between the maximum electric field vectors. Only that part of $\mathbf{E}(t)_{sum}$ which rotates inphase with the ion's velocity vector is effective in accelerating the ions. That is, $\mathbf{E}^{+}(t)$ corresponds to the inphase accelerating contribution and an ion rotating inphase with $\mathbf{E}^{+}(t)$ is accelerated to a larger cyclotron radius.

The effect of excitation on ions which are out of phase is illustrated in Figure 1. An ion which has a velocity vector that is inphase with respect to the electric field (A) is accelerated resulting in an increase in the cyclotron radius. Conversely, ion motion (B) that is out of phase with respect to the electric field results in deceleration and a smaller radius of the cyclotron orbit (*40*, *42–44*).

The effect of phase angle on ion excitation can be observed in a two-section cell by utilizing the conductance limit orifice as an ion skimmer (*39*, *40*). The experimental procedure is illustrated in Figure 2. Following the ionization pulse, all ions are accelerated by using frequency swept excitation until the radius of the ion's cyclotron orbit is larger than the radius of the aperture of the conductance limit. Following the initial excitation (S1), a delay is introduced to allow the phase of a second rf excitation (S2) to vary with respect to the phase of the ion packet. Thus, the phase relationship between S1 and S2 is a function of the delay. If S2 is initiated following a delay corresponding to $(N/2)\tau$ (N = 2, 4, 6, ... and τ is the period of the cyclotron orbit) the second excitation will be inphase with the ion motion (see Figure 2A), whereas a delay corresponding to $(N/2)\tau$ (N = 1, 3, 5, ...) shifts the phase of the second excite pulse by 180° and the ions are decelerated (Figure 2B) resulting in a reduction of the radius of the ion's

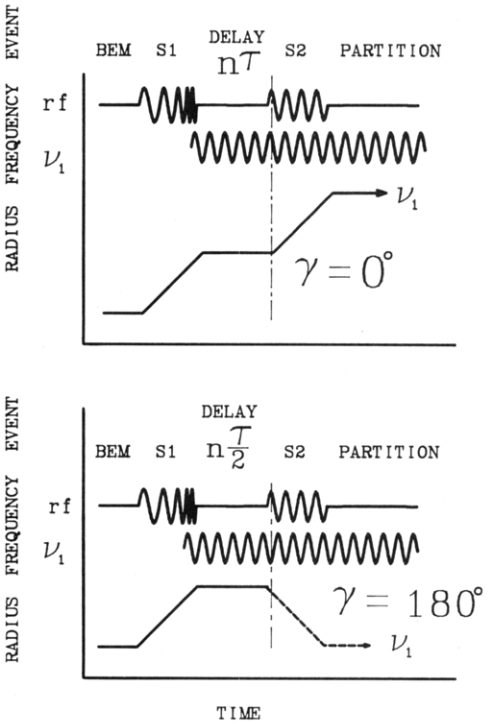

Figure 2. Phase angle of an ion's motion with respect to the applied rf excitation determined by a delay between two distinct excite pulses. A delay corresponding to an integral number of cyclotron periods (τ) results in a second excitation which is inphase with the ion motion. Conversely, a delay corresponding to an integral number of $\tau/2$ produces an out-of-phase excitation resulting in a decrease of the cyclotron radius.

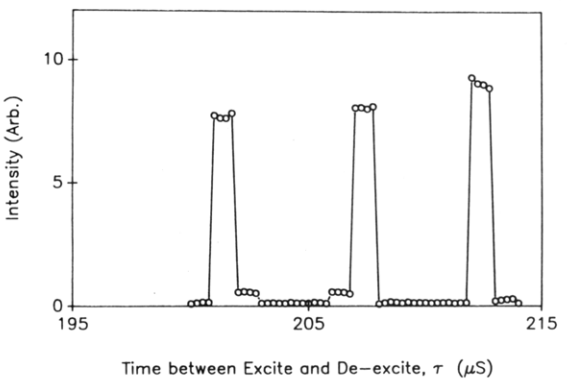

Figure 3. Effect of phase angle on excitation observed by monitoring partitioning efficiency of $I_2^{+\bullet}$ as a function of a phase delay between two excite pulses. The maxima in the plot correspond to delays which correspond to out-of-phase deceleration of the ion ensemble to radii that can be partitioned form the source to analyzer region.

cyclotron orbit. *Only* ions which are de-excited by out-of-phase excitation can be partitioned into the analyzer region, and the ion intensity observed in the analyzer region is a measure of the partitioning efficiency (*40*).

To illustrate the dependence of excitation on the phase angle, $I_2^{+\bullet}$ was formed in the source region, partitioned, and detected in the analyzer region. Prior to partitioning from the source to analyzer regions, the ions are accelerated (120 V/m, 250 μs) to sufficiently large cyclotron radii such that ion partitioning cannot occur. The radii of these ions are then further modulated by a second excitation (120 V/m, 250 μs). The phase of the second excitation is determined by a variable time delay between the two excite pulses. Contained in Figure 3 is a plot of signal intensity (m/z 254 in the analyzer region) versus the period between the first and second excite pulses. The maxima correspond to I_2 being de-excited to smaller radii by an out-of-phase second excitation. Because the relative

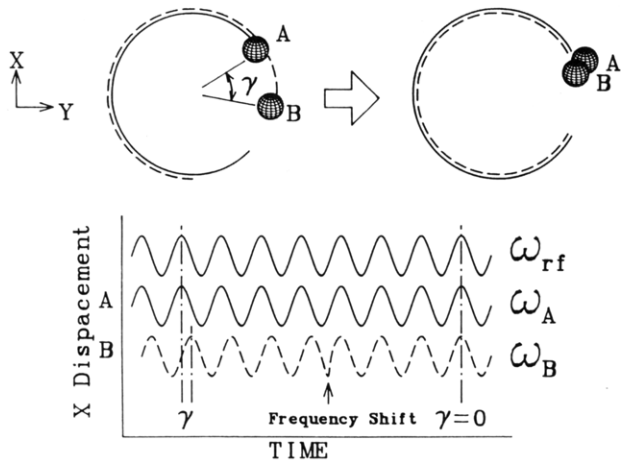

Figure 4. Two ions (I and II) having the same frequency but different phases ($\gamma = 0$) can only be driven into phase coherence ($\gamma = 0$) by shifting the frequency of the out-of-phase ion.

phases of the ion motion and second excitation pulse are shifted by 180° once every period, the period between the maxima is ca. 5.5 μs (the period of the cyclotron orbit of m/z 254). The narrow peak width observed in the phase-specific partitioning of iodine demonstrates the significance of the relative phase of ion motion with respect to the applied excitation. It is apparent that excitation and de-excitation are strongly phase dependent because molecular iodine is *only* partitioned during discrete time intervals (i.e., narrow phase distribution). It should be noted that the phase-specific scheme of separating ions requires ion packets of small radial and angular distribution with respect to the FT-ICR cell. That is, ions must be formed with low kinetic energies in the $X-Y$ plane (e.g. electron impact ionization) such that they can be "driven" into phase coherence. Only ion packets having well-defined phase coherence give rise to phase-specific excitation/de-excitation of the entire ion ensemble. It should be noted that sample pressures were maintained at 2×10^{-7} Torr or lower in order to minimize adverse effects caused by ion–neutral collisions (*45*).

Owing to the strong dependence of ion acceleration on phase angle, it is necessary to "drive" ions having initially random phase angles into synchronous alignment with the rf electric field prior to a net gain of translational energy (*41*). Phase advancement is the mechanism whereby ions having initially random phases are advanced into synchronous motion with the applied resonant rf field. Illustrated in Figure 4 are the frequencies generated by the motion of two ions relative to a resonant rf electric field. In the figure, ion I is initially inphase with the applied rf field and ion II is initially shifted by a phase angle γ. In order for the relative phase of ion II to be "driven" into phase with ion I and the applied rf electric field, the period of the cyclotron orbit (and therefore frequency) of ion II must be changed. An essential feature of ICR is that the cyclotron frequency is related to the mass-to-charge ratio of the ion and the magnetic field strength and *independent* of the translational energy of the ion. Acceleration of an ion in a magnetic field results in a larger cyclotron radius and *not* in a change in frequency.

The frequency shift required to move an out-of-phase ion into synchronous alignment with the applied electric field is illustrated by evaluating the forces affecting ion motion. As shown in Figure 5, the orbit of an ion (I) which is in continuous alignment with a resonant rf electric field ($\omega_{rf} = \omega_c$) is described by the Lorentz force (F_L) balanced by the centrifugal force (F_C). Because the force applied by the electric field (F_E) is perpendicular to both F_L and F_C, the effect of F_E on the angular frequency of ion I is zero and the angular frequency

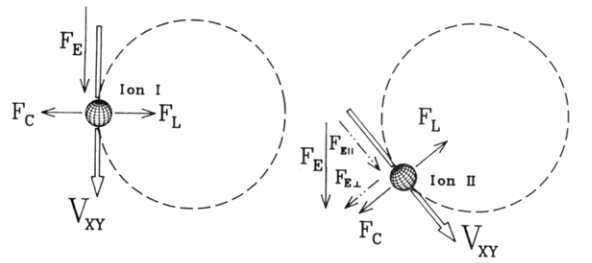

Figure 5. Angular frequency of an ion determined by balancing the radially outward forces with the radially inward forces. Thus, the frequency of an ion which is out of phase with respect to an applied rf electric field is different than an ion which is inphase (ω_c) due to a perpendicular component of the applied electric field ($F_{E\perp}$). Such differences in the frequencies allows the out-of-phase ion to phase advance.

(ω_I) is obtained by equating the Lorentz and centrifugal forces (see eq 4).

$$(mv^2)/r = qvB \tag{4}$$

and

$$\omega_I = v/r = qB/m = \omega_c$$

Conversely, an ion that is out of phase with E_{rf} is affected by both parallel and perpendicular components of the electric field. Therefore, the orbit of the out-of-phase ion II is obtained by equating the total outward radial force ($F_C + F_{E\perp}$, where $F_{E\perp} = qE_\perp = qE \sin \gamma$ in Figure 5) with F_L. Thus

$$(mv^2)/r + qE_\perp = qvB \tag{5}$$

and

$$\omega_{II} = \frac{v}{r} = \frac{qvB - qE_\perp}{mv} < \omega_c \tag{6}$$

If ion II is accelerated by an rf electric field having a frequency equal to the *natural* cyclotron frequency of ion II ($\omega_{rf} = \omega_c = qB/m$), the ion motion and the rf electric field will have different frequencies. Because ω_{II} is a discrete frequency compared to ω_{rf}, the relative phase angle (between ω_{II} and ω_{rf}) changes. It can be seen from eq 6 that $\omega_{rf} > \omega_{II}$, allowing the phase of the applied rf electric field to align with the phase of ion II (initially leading the rf electric field by γ in Figure 5). Conversely, if ion II has a phase angle equivalent to $-\gamma$ (i.e., $\gamma = 181°–359°$), ω_{II} would be increased by $+qE_\perp$, allowing the ion to advance into phase with the applied rf electric field. As the relative phase angle (γ) approaches zero, ω_{II} approaches ω_{rf} dur to the alignment of the electric field with the ion motion. When $E_\perp = 0$, there is no component of the electric field radially outward and $\omega_{II} = \omega_{rf}$. Thus, ion II remains both resonant and inphase with the applied rf electric field following phase advancement.

In the case where $F_{E\perp}$ is initially negligible with respect to F_L (i.e., $qvB \gg qE_\perp$), the frequency shift of ion II caused by the misalignment of the electric field is also small; thus $\omega_{II} \approx \omega_c$. Under these initial conditions the time required for phase advancement (τ_{phase}) of ion II is increased due to the relative force of the magnetic field. Rapid phase synchronization occurs under conditions where the perpendicular component of the applied electric field is significant with respect to the force of the magnetic field. Because the force of the magnetic field is velocity dependent, the relative force on an ion by qvB and $qE_\perp$ is also velocity dependent. Therefore, phase advancement occurs more quickly for low-velocity ions.

As shown in Figure 1, an ion that is 180° out of phase will have no perpendicular component of the applied rf electric field. Because the frequency of the out-of-phase ion is the same as the natural cyclotron motion of the ion (i.e., the frequency of the applied rf electric field), phase advancement

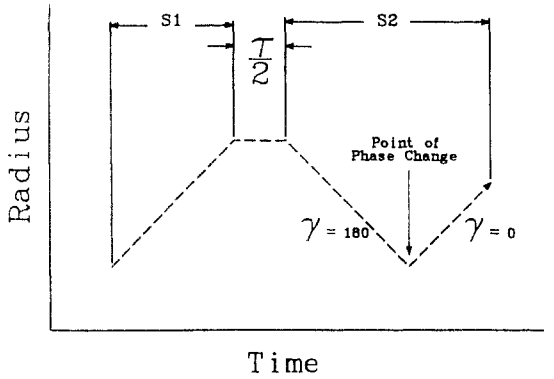

Figure 6. Plot of ion radius versus time. An ion that is decelerated by a second excitation pulse undergoes phase advancement. Following phase synchronization, the ion gains translational energy due to the resonant excitation resulting in a larger cyclotron radius.

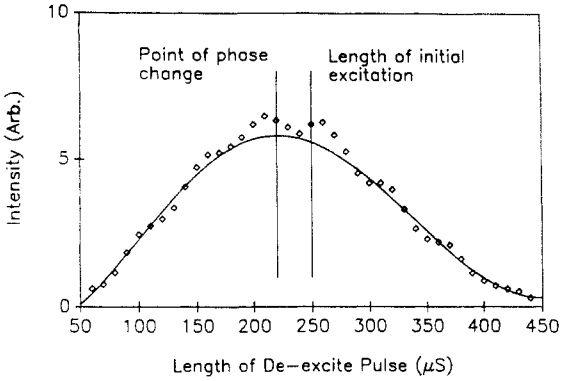

Figure 7. Plot of intensity of $I_2^{+\bullet}$ following partitioning as a function of the de-excitation period (S2) subsequent to a 250-μs inphase acceleration. The translational energy of the ion undergoing phase advancement is determined by the difference between the initial energy of the ion and the energy required to reduce its velocity to the point of phase synchronization.

does not occur and the ion remains out of phase. A continuous misalignment of the rf electric field with respect to an ion's velocity vector results in deceleration and not phase synchronization. Such an ion is decelerated to a velocity where the force of the electric field is strong with respect to the magnetic field. Under these conditions the ion undergoes phase advancement and moves synchronously with the electric field (*46*).

The radial velocity of an ion undergoing phase advancement can be determined experimentally in a two-section cell. The sequence used to investigate the radial velocity of an ion during phase advancement is illustrated in Figure 6. Following the ionization pulse, ions of a given m/z value are accelerated to larger cyclotron radii by an rf pulse. The ions are decelerated by a second rf excitation pulse following a delay corresponding to a 180° phase shift. The radius of the out-of-phase ions is reduced until the ions are decelerated to a velocity at which the electric field is no longer negligible. At this interface the ions are "driven" into phase. Following phase synchronization, the ion's radial velocity (radius) increases due to inphase rf excitation.

The radial velocity of $I_2^{+\bullet}$ at the point of phase advancement is determined by observing the signal intensity of ions partitioned from source to analyzer regions as a function of the length of the de-excite pulse (see Figure 7). Only ions that are decelerated to radii smaller than the dimensions of the conductance limit are partitioned and observed in the analyzer region. Conversely, ions that are decelerated below the velocity for phase advancement become inphase with ω_{rf} and subsequently gain radial velocity. Ions that gain energy following phase advancement are accelerated to radii sufficiently large to prohibit partitioning. Therefore, the maximum signal intensity of $I_2^{+\bullet}$ observed in the analyzer region corresponds to the minimum energy (i.e., smallest radius). Because the minimum energy during the deceleration process corresponds to the radial velocity of the ion undergoing phase advancement, the maximum intensity can be related to the velocity at which phase advancement occurs.

The maximum in the plot contained in Figure 7 occurred after ca. 225 μs of rf excitation. Because the initial excitation was 250 μs in length, the difference between the two excitation times can be related to the energy of $I_2^{+\bullet}$ undergoing phase advancement. $I_2^{+\bullet}$ gained ca. 30 eV of energy during the first excitation pulse. Because the energy which was removed by the second excitation corresponds to ca. 25 eV, the energy at which phase advancement occurs is ca. 5 eV.

Phase advancement occurs as $F_{E\perp}$ increases with respect to F_L; therefore, the length of the de-excitation period is a function of the difference in the initial angular velocity of an ion (v_o/r) to the angular velocity at which the ion phase advances. Further, ions which are stored in the ion cell with greater than thermal translational energies must interact with the rf excitation for a period of many cyclotron orbits prior to advancing into synchronous motion. Maximum acceleration occurs when the ion's velocity vector is synchronous with the applied excitation. It is important to note that the total excitation time (τ_{total}) of the ion ensemble is limited by the time that an inphase ion can be accelerated prior to ejection from the ICR cell. Because τ_{total} is constant for all ions regardless of phase, different times required for phase advancement (τ_{phase}) result in differences in the net period of excitation of the individual ions of the ensemble

$$\tau_{net} = \tau_{total} - \tau_{phase}$$

The effect of initial radial velocity on the final dimensions of the ion packet has been simulated by trajectory calculations (*41*). Ion location is determined by calculating the resultant vectors of the electric and magnetic fields. This procedure is used to study the effects of individual factors (i.e., initial kinetic energy) on ion motion. The effects of initial angular velocity on phase synchronization are illustrated by observing the effect of rf excitation for an ion that is initially inphase ($\gamma = 0$) compared to that of an ion that is initially out of phase ($\gamma = 180$). Figure 8A contains a temporal plot of the calculated trajectories for two ions (m/z 500) having thermal kinetic energies and a relative phase angle of 180°. The trajectories result from acceleration of the ions with a resonant, single frequency rf field (900 v/m). Because the initial radial velocity is low, $F_L \approx F_{E\perp}$, phase advancement and phase synchronization occur quickly and the ions are excited as a coherent packet. Conversely, ions which have initial radial velocities corresponding to 3 eV of kinetic energies follow markedly different trajectories (see Figure 8B). Because $F_L > F_{E\perp}$, the ion which is out of phase experiences a continuous misalignment with the electric field resulting in a different trajectory compared to that of an ion which is initially inphase. The simulations show that instantaneous phase synchronization prior to a net gain of translational energy results in better spatial definition of the ion ensemble following excitation. The spatial distribution of the ion packet following excitation is defined by the relative differences in the temporal locations of the ions comprising the ion ensemble. For example, the ions having well-defined (i.e., coherent) dimensions have negligible differences in their temporal positions relative to the average radius of the ensemble.

Ions which are produced by electron impact have initial velocities which correspond to the translational energies of the neutrals prior to ionization. Owing to the low initial radial velocity of the ions produced, phase advancement of out-of-phase ions occurs quickly and the final radial distribution is

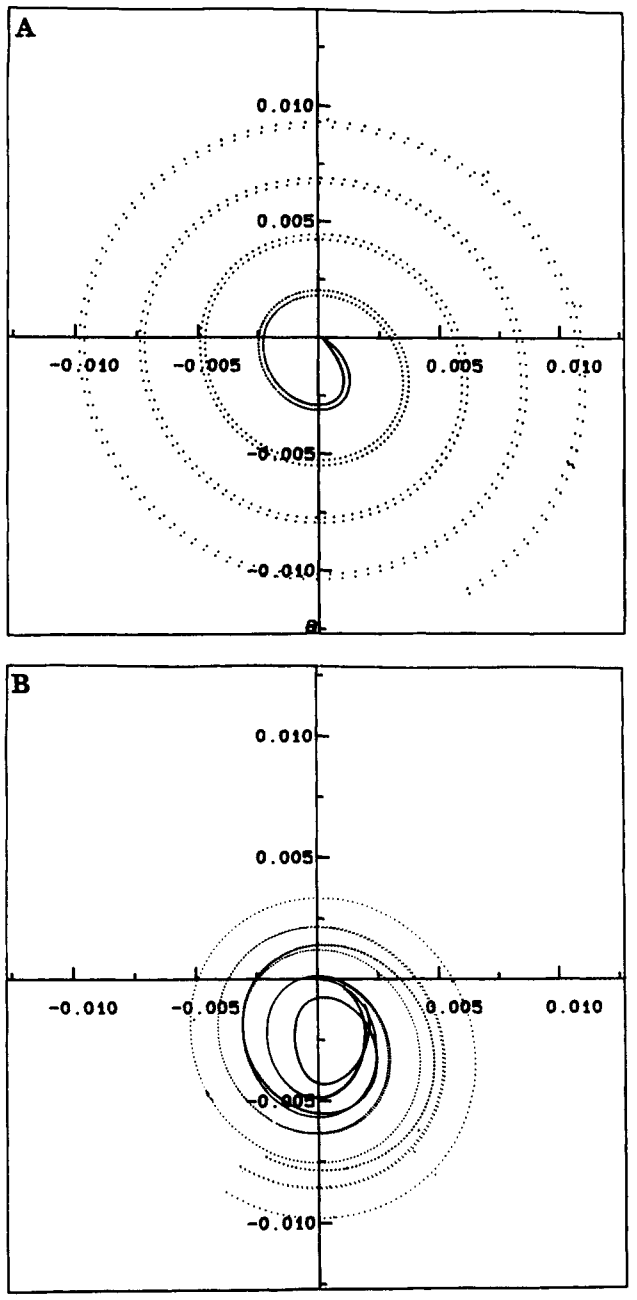

Figure 8. Temporal plots of ion location determined by numerical solution of the equations of ion motion for (A) ions having initially thermal translational energies (0.05 eV) and (B) ions having significant (3 eV) initial radial translational energies. The effect of initial radial velocity on packet coherence following excitation is illustrated by comparing the different trajectories for two ions which are phase shifted by 180°.

small with respect to the radius after excitation. The initial dimensions of the ion population produced by electron impact correspond to the dimensions of the electron beam in the $X-Y$ plane and in the Z direction by the location of the electrostatic trap plates. Diffusion of the ions into the $X-Y$ plane is a function of the ion density and the magnetic field strength. In the absence of space charge effects the diffusion of the ion population into the $X-Y$ plane is also negligible. Because the initial spatial distribution is small and the ion's radial velocity is low, the distribution of cyclotron orbit centers is also small. Conversely, ions which are injected into the ion cell from an external source are given sufficient translational energies to move the ions from the source to analyzer regions. The initial dimensions of the ion population created by ion injection correspond to the focusing characteristics of the ion optics. Optics that have substantial focusing characteristics in the $X-Y$ plane or produce fringing fields cause redirection of ion velocity into the $X-Y$ plane (*47*). Therefore, injected ions acquire translational energies of several orders of magnitudes greater than the translational energies of ions which rapidly undergo phase synchronization. The time required for deceleration of ions by out-of-phase excitation produces a significant final radial distribution following excitation of the ensemble of ions.

CONCLUSIONS

As illustrated in the preceding section, rapid phase synchronization of ions is achieved in excitation fields where $F_{E\perp} > F_L$. The high power required to generate an electric field of this magnitude is difficult to use because of the poorly defined excitation field lines which result from cubic ICR cells. It has been shown that ion evaporation along the Z axis occurs as a result of excitation fields which have components of the electric field vectors in the Z direction (*48*, *49*). During high-power excitation, significant electric field gradients are produced along the Z axis which lead to loss of sensitivity (*50*, *51*).

Although phase advancement of ions can occur quickly (i.e., within the period of a single orbit) in excitation fields where $F_{E\perp} > F_L$, phase synchronization occurs over many cyclotron periods in weaker excitation fields. Therefore, phase synchronization can be achieved by long irradiation times during which ions have sufficient time to interact with the rf field. Phase synchronization caused by long irradiation times selectively discriminates against high mass ions. Because the dimensions of the cyclotron radius are dependent on both angular velocity in the $X-Y$ plane and the mass of the ion, high mass ions absorb less energy before being ejected from the ion cell. Thus, the impact of phase synchronization of the ion packet increases with m/z ratio.

The initial distribution of cyclotron orbit centers is a function of radial velocity and m/z ratio. Because the radius of the cyclotron orbit is directly dependent on both the angular velocity in the $X-Y$ plane and the m/z ratio of the ion, high mass ions injected from an external ion source result in a poorly defined distribution of orbit centers. As a result of the initial spatial distribution, significant initial radial velocities, and the inability to phase advance, it becomes increasingly difficult to produce a coherent packet of high mass ions.

Ion detection by FT-ICR is dependent on the production and detection of a well-defined ion ensemble. The inability to produce a spatially defined cycloiding ion packet results in the loss of the expected performance characteristics. For example, the detected image current is directly dependent on the number of ions in the packet and the distance that the packet is from the detection plate. An energy distribution caused by initially high radial velocities and random phases reduces the interaction of the low-energy ions with the receive plates of the ICR cell. Thus, an ion packet which has poor spatial definition suffers loss of sensitivity. In the case of low abundance biomolecules, further signal loss due to other mechanisms for ion evaporation can lead to rapid loss of the time-domain transient signal (i.e., loss of resolution).

ACKNOWLEDGMENT

We wish to thank Dr. R. Kenefick and S. Cornford for many helpful discussions.

LITERATURE CITED

(1) Gross, M. L.; Rempel, D. L. *Science* **1984**, *226*, 261.
(2) Wilkins, C. L.; Gross, M. L. *Anal. Chem.* **1981**, *53*, 1661A.
(3) Russell, D. H. *Mass Spectrom. Rev.* **1986**, *5*, 167–189.
(4) Wanczek, K. P. *Int. J. Mass Spectrom. Ion Processes*, in press.
(5) Marshall, A. G. *Acc. Chem. Res.* **1985**, *18*, 316–322.
(6) Laude, D. A.; Johlman, C. L.; Brown, R. S.; Wiel, D. A.; Wilkins, C. L. *Mass Spectrom. Rev.* **1986**, *5*, 107–166.
(7) Buchanan, M. V.; Comisarow, M. B. In *Fourier Transform Mass Spectrometry: Evolution, Innovation, and Applications*; ACS Symp. Series

359; Buchanan, M. V., Ed.; American Chemical Society: Washington, DC, 1987; pp 1–20.
(8) Nibbering, N. M. M. *Adv. Phys. Org.* **1988**, *24*, 1.
(9) Freiser, B. S. In *Techniques for the Study of Ion Molecule Reactions*; Farrar, J. M., Saunders, W., Eds.; Wiley: New York, 1988.
(10) Hanson, C. D.; Kerley, E. L.; Russell, D. H. In *Treatise on Analytical Chemistry*, 2nd ed.; Wiley: New York, 1988; Vol. 11, Chapter 2.
(11) Hunt, D. F.; Shabanowitz, J.; Yates, J. R.; Russell, D. H.; Castro, M. E. *Proc. Natl. Acad. Sci. U.S.A.* **1987**, *84*, 620.
(12) Ijames, C. F.; Wilkins, C. L. *J. Am. Chem. Soc.* **1988**, *110*, 2687.
(13) Dunbar, R. C. *Molecular Ions: Spectroscopy, Structure and Chemistry*; North Holland: Amsterdam, 1983; p 231.
(14) Carlin, T. J.; Freiser, B. S. *Anal Chem.* **1983**, *55*, 571.
(15) Bricker, D. L.; Adams, T. A.; Russell, D. H. *Anal. Chem.* **1983**, *55*, 2417.
(16) Anders, L. R.; Beauchamp, J. L.; Dunbar, R. C.; Baldeschwieler, J. D. *J. Chem. Phys.* **1966**, *45*, 1062.
(17) Sommer, H.; Thomas, H. A.; Hipple, J. A. *Phys. Rev.* **1951**, *82*, 697; **1949**, *76*, 1877; **1950**, *78*, 806; **1950**, *80*, 487.
(18) Sommer, H.; Thomas, H. A.; Hipple, J. A. *Phys. Rev.* **1949**, *76*, 1877.
(19) Sommer, H.; Thomas, H. A.; Hipple, J. A. *Phys. Rev.* **1950**, *80*, 487.
(20) Barber, M.; Bordoli, R. S.; Elliot, G. J.; Sedgwick, R. D.; Tyler, A. N. *Anal. Chem.* **1982**, *54*, 645A.
(21) Benninghoven, A.; Jaspers, D.; Sichtermann *Appl. Phys.* **1976**, *11*, 35.
(22) Posthumus, M. A.; Kistemaker, P. G.; Meuzelaar, H. L. C.; TenNoever de Brauw, M. C. *Anal. Chem.* **1978**, *50*, 985.
(23) McCrery, D. A.; Ledford, E. B.; Gross, M. L. *Anal. Chem.* **1982**, *54*, 1437.
(24) Castro, M. E.; Russell, D. H. *Anal. Chem.* **1984**, *56*, 578.
(25) Comisarow, M. B.; Marshall, A. G. *Chem. Phys. Lett.* **1974**, *25*, 282.
(26) Marshall, A. G.; Comisarow, M. B.; Parisod, G. *J. Chem.* Phys. **1979**, *71*, 4434–4444.
(27) Wilkins, C. L.; Gross, M. L. *Anal. Chem.* **1981**, *53*, 1661A.
(28) Hanson, C. D.; Castro, M. E.; Russell, Hunt, D. F.; Shabanowitz, J. In *Fourier Transform Mass Spectrometry: Evolution, Innovation, and Applications*; Buchanan, M. V., Ed.; ACS Symposium Series 359; American Chemical Society: Washington, DC, 1987; pp. 100–115.
(29) Grese, R. P.; Rempel, D. L.; Gross, M. L. In *Fourier Transform Mass Spectrometry: Evolution, Innovation, and Applications*; Buchanan, M. V. Ed.; ACS Symposium Series 359, American Chemical Society: Washington, DC, 1987; pp 34–59.
(30) Ledford, E. B.; Rempel, D. L.; Gross, M. L. *Anal. Chem.* **1984**, *56*, 2744–2748.
(31) Rempel, D. L.; Huang, S. K.; Gross, M. L. *Int. J. Mass Spectrom. Ion Processes* **1986**, *70*, 163–184.
(32) Comisarow, M. B.; Marshall, A. G. *J. Chem. Phys.* **1976**, *64*, 110.
(33) Marshall, A. G. *Anal. Chem.* **1979**, *51*, 1710.
(34) McIver, R. T.; Ledford, E. B.; Hunter, R. L. *J. Chem. Phys.* **1980**, *72*, 2535.
(35) Buttrill, S. E. *J. Chem. Phys.* **1969**, *50*, 5690.
(36) Beauchamp, J. L. *J. Chem. Phys.* **1967**, *46*, 1231.
(37) Marshall, A. G. *J. Chem. Phys.* **1971**, *55*, 1343–1354.
(38) Ghaderi, S.; Littlejohn, D. In *Proceedings of the 33rd Annual Conference on Mass Spectrometry and Allied Topics, San Diego*; American Society for Mass Spectrometry, 1984; p 727.
(39) Kerley, E. L.; Russell, D. H. *Anal. Chem.* **1989**, *61*, 53–57.
(40) Hanson, C. D.; Kerley, E. L.; Russell, D. H. *Anal. Chem.* **1989**, *61*, 83–85.
(41) Baykut, G.; Watson, C. H.; Eyler, J. R. In *Proceedings of the 36th Annual Conference on Mass Spectrometry and Allied Topics, Denver*; American Society for Mass Spectrometry, 1987; pp 387–388.
(42) Marshall, A. G.; Wang, T. L.; Ricca, T. L. *Chem. Phys. Lett.* **1984**, *105*, 233.
(43) Pfandler, P.; Bodenhausen, G.; Rapin, J.; Houriet, R.; Gaumann, T. *Chem. Phys. Lett.* **1987**, *138*, 195.
(44) Hanson, C. D.; Kerley, E. L.; Castro, M. E.; Russell, D. H. In *Proceedings of the 37th Annual Conference on Mass Spectrometry and Allied Topics, San Francisco*; American Society for Mass Spectrometry, 1988; p 612.
(45) Kerley, E. L.; Hanson, C. D.; Russell, D. H., unpublished results at Texas A&M University, 1989.
(46) McIver, R. T.; Hunter, R. L.; Baykut, G. *Anal. Chem.* **1989**, *61*, 489.
(47) Kerley, E. L.; Hanson, C. D.; Castro, M. E.; Russell, D. H., manuscript in preparation, to be submitted to *Anal. Chem.*
(48) Huang, S. K.; Rempel, D. L.; Gross, M. L. *Int. J. Mass Spectrom. Ion Processes* **1986**, *72*, 15.
(49) Kofel, P. M.; Allemann, M.; Kellerhals, Hp.; Wanczek, K. P. *Int. J. Mass Spectrom. Ion Processes* **1985**, *65*, 97.
(50) van der Hart, W. J.; van de Guchte, W. J. *Int. J. Mass Spectrom. Ion Processes* **1988**, *82*, 17.
(51) Shabanowitz, J., personal communication.

RECEIVED for review December 2, 1988. Accepted May 30, 1989. This work was supported by the National Institutes of Health–General Medical Sciences (GM-33780) and the National Science Foundation (CHE-8418457). Some of the equipment was purchased from funds provided by the TAMU Center for Energy and Mineral Resources. We gratefully acknowledge the Texas Agricultural Experiment Station for providing a portion of the funds for purchase of the Nicolet FTMS 1000 mass spectrometer.